Bistable chaos. II. Bifurcation analysis

M. G. M. Gomes and G. P. King

Nonlinear Systems Laboratory, Mathematics Institute, University of Warwick, Coventry CV4 7AL, United Kingdom

Results of a bifurcation analysis are given for the model of a Van der Pol–Duffing autonomous electronic oscillator. The oscillator is described by three ordinary differential equations and consists of a RC oscillator resistively coupled to an LC oscillator. The steady-state problem is described by the unfolding of the quartic potential $F = \frac{1}{4}X^4 - \frac{1}{2}\alpha X^2 + \mu X$, giving rise to the elementary cusp catastrophe. We show how the bifurcation diagram evolves with μ and recover a "cross-shaped diagram" reminiscent of the one obtained by Boissonade and De Kepper for the Belousov-Zhabotinskii chemical system [J. Phys. Chem. **84**, 501 (1980)]. We also show that nonzero values of μ result in coexisting attractors with different dynamics. Specifically, we show a limit cycle attractor in one potential well coexisting with a chaotic attractor in the other well.

PACS number(s): 02.50.+s, 05.40.+j, 05.45.+b

I. INTRODUCTION

In this paper, we describe the bifurcation phenomena arising in the circuit equations modelling the *chaotic Van der Pol–Duffing oscillator* shown in Fig. 1. The bifurcations and dynamics in this oscillator are due to the presence of the nonlinear negative resistor N whose I-V characteristic we model with the polynomial

$$I_N(V) = \nu + aV + bV^3, \qquad (1.1)$$

where $a < 0$ and $b > 0$.

Previous investigations of this circuit and its variants have assumed $\nu = 0$ and reported the main bifurcation sequence shown in Fig. 2(a) [1–4]. The main sequence is obtained by following a suitably chosen parameter path in the (a, r^{-1}) plane (r is defined in Fig. 1). The sequence begins with a symmetry-breaking transition (via a pitchfork bifurcation) from S^0 to the *conjugate* attractors S^+ and S^-. Both attractors undergo a Hopf bifurcation followed by a sequence of period-doubling bifurcations to chaos. The bifurcations from the S^+ and S^- branches occur at the *same* parameter values. This region of bistability ends with a *symmetry-increasing* bifurcation [5, 6] (via a crisis) to a single chaotic attractor C^0. A one-parameter family of the described bifurcation sequences is expected to contain an element for which the pitchfork and Hopf bifurcations occur at the same parameter value. This bifurcation has generically codimension-2 and it has first been described by Takens [7,8] and Bogdanov [9]. It is known as a Takens-Bogdanov (TB) bifurcation.
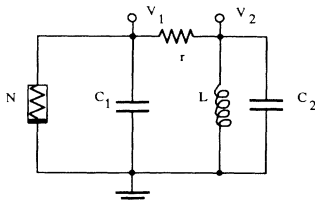
The above bifurcation sequence possesses reflectional or $\mathcal{Z}_2$ symmetry and is not preserved by small perturbations (i.e., it is *nongeneric*). It is nongeneric because the pitchfork bifurcation from S^0 to $S^{\pm}$ is nongeneric. Physically this means that small symmetry-breaking effects are present and corresponds to $\nu \neq 0$ in model (1.1). The generic picture for the pitchfork is given by the elementary cusp catastrophe. In this paper we show that the presence of the cusp catastrophe in the steady-state problem gives rise to the bifurcation sequence shown in Fig. 2(b).

The paper is organized as follows. In Sec. II we describe three nonlinear circuits obtained as limiting cases of Fig. 1, and the TB singularity since it plays an essential role in later sections. We also show that the equations for one of the circuits can be transformed into the model used by Boissonade and De Kepper [14] to interpret bistability and oscillations for chemical reactions in continuously stirred tank reactors.

In Secs. III and IV, we give our analytic and numerical results for the chaotic Van der Pol oscillator. In Sec. III results for the symmetric system ($\mu = 0$) are given. We

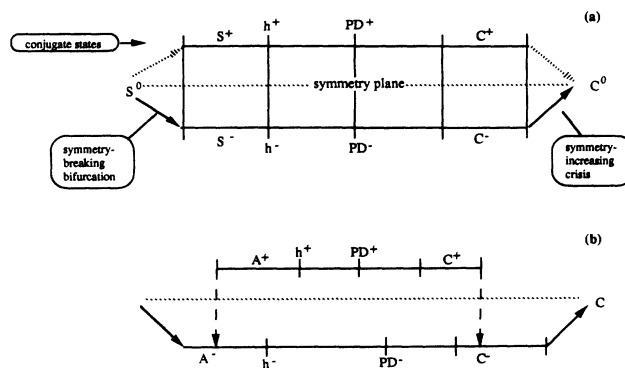FIG. 1. Circuit diagram for a chaotic Van der Pol–Duffing oscillator.

FIG. 2. Main bifurcation sequences obtained along a curve in the (a, r^{-1}) plane: (a) symmetric bifurcation sequence ($\nu = 0$); (b) asymmetric bifurcation sequence ($\nu \neq 0$).

find a TB line of codimension-2 in the parameter space. This line contains a degenerate point of codimension-3 where a change of stability occurs. As described in Guckenheimer and Holmes [10], several codimension-1 bifurcations (pitchfork, Hopf, homoclinic, saddle node of limit cycles when $\mathscr{Z}_2$ symmetry is assumed) meet at a codimension-2 degeneracy of the TB type. Homoclinic bifurcations and saddle node of limit cycles are global bifurcations and as such they require numerical methods to be tracked away from a small neighborhood of the codimension-2 point. In our numerical experiments the value of one of the parameters has been fixed so that we are left with a two-dimensional parameter space that intersects transversally the TB line. In Sec. IV, we use numerical simulations to obtain a bifurcation set for the asymmetric system. Again one of the parameters is fixed (the same as in Sec. III). Now we are left with a three-dimensional parameter space that intersects transversally a TB cusped sheet. The bifurcation set will be described by restricting to several two-dimensional sections.

Finally we give our conclusions in Sec. V.

II. CIRCUITS AND SINGULARITIES

In this section we describe three limiting cases of circuit 1. By analyzing the model equations we find singularities that are also present in the chaotic Van der Pol–Duffing oscillator. There is a considerable advantage to this approach. By taking the limits we get simpler systems. Some of the complicated behavior of circuit 1 is no longer present, which makes easier the concentration on the singularities. Altogether these limits give a good intuition for what is going to happen in the full system and, furthermore, introduce some machinery in an organized way.

A. Limiting cases

The three nonlinear circuits shown in Fig. 3 are obtained as limiting cases of Fig. 1. The circuit equation for Fig. 3(a) is

$$\dot{V}_1 = -\frac{1}{C_1}\left(bV_1^3 + aV_1 + \nu\right)$$

which may also be written as

$$\dot{V}_1 = -\frac{1}{C_1}\frac{dF}{dV_1},$$

where F is the potential

$$F(V_1) = \tfrac{1}{4}bV_1^4 + \tfrac{1}{2}aV_1^2 + \nu V_1.$$

The steady states of this circuit are completely characterized by the canonical cusp catastrophe.

We recall some results from elementary catastrophe theory [11]. Given the potential F, the *equilibrium manifold* M is defined by the equation

$$\nabla_x F = 0,$$

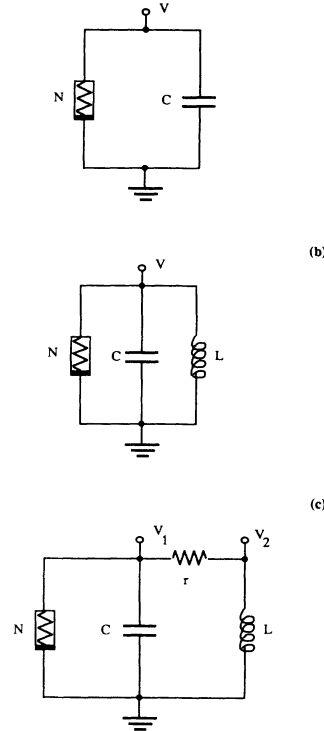where the subscript x indicates that the gradient is with

FIG. 3. Three nonlinear circuits embedded in the chaotic Van der Pol–Duffing circuit: (a) nonlinear RC circuit; (b) Van der Pol oscillator; (c) Van der Pol–Duffing oscillator.

respect to the state variables. In the present case this yields for M the equation

$$bV_1^3 + aV_1 + \nu = 0.$$

By varying the *control* parameters a and ν the familiar folded surface of the canonical cusp catastrophe manifold may be generated. The folds of this surface when projected onto the (a, ν) plane yield the cusp

$$b\left(\frac{\nu}{2}\right)^2 = \left(\frac{-a}{3}\right)^3.$$

Inside the cusp the potential F has two minima whose relative depth is determined by ν. In this region the system is said to be *bistable*.

The circuit in Fig. 3(b) is a Van der Pol oscillator and may be obtained from Fig. 1 either by setting $C_1 = 0$ or $r = 0$. Assuming $r = 0$ yields Van der Pol's equation

$$\dot{V}_1 = -\frac{1}{C_1}\left(bV_1^3 + aV_1 + \nu + I_L\right),$$

$$\dot{I}_L = \frac{1}{L}V_1,$$

which in more familiar form is

$$\ddot{V}_1 + \frac{1}{C_1}\left(a + 3bV_1^2\right)\dot{V}_1 + \frac{1}{LC_1}V_1 = 0.$$

The bistability present in the previous circuit has disappeared (but see Zeeman [12] for a catastrophe theory interpretation).

The circuit in Fig. 3(c) is a Van der Pol–Duffing oscillator. The circuit equations are

$$\dot{V_1} = -\frac{1}{C_1}\left(bV_1^3 + aV_1 + I_L + \nu\right),$$

$$\dot{I_L} = \frac{V_1}{L} - \frac{r}{L}I_L. \tag{2.1}$$

The reader will note that there is little difference between the circuits of Figs. 3(b) and 3(c). Nevertheless the introduction of the resistor r has a profound effect: Not only is bistability recovered but, as will be shown below, we also have a cusped curve of TB codimension-2 bifurcations (TB cusp).

B. A Takens-Bogdanov cusp

Before discussing system (2.1) further, we bring it into dimensionless form with the scaling

$$X = \sqrt{\frac{bL}{rC_1}}V_1, \qquad Z = \sqrt{\frac{bLr}{C_1}}I_L, \qquad \tau = \frac{r}{L}t,$$

which yields the system

$$\dot{X} = -(X^3 - \alpha X + \mu) - \Gamma Z,$$

$$\dot{Z} = X - Z, \tag{2.2}$$

where differentiation is with respect to τ and the three parameters are

$$\alpha = \frac{-L}{rC_1}a, \mu = \sqrt{\frac{bL^3}{r^3C_1^3}}\nu, \text{ and } \Gamma = \frac{L}{r^2C_1}.$$

For ease of interpretation we write system (2.2) as the second-order equation

$$\ddot{X} + \left[-(\alpha - 1) + 3X^2\right]\dot{X} + \frac{\partial F}{\partial X} = 0, \tag{2.3}$$

where F is the potential

$$F(X) = \tfrac{1}{4}X^4 - \tfrac{1}{2}(\alpha - \Gamma)X^2 + \mu X. \tag{2.4}$$

When $\mu = 0$ the potential F has one minima for $\alpha < \Gamma$ and two minima of equal depth for $\alpha > \Gamma$. In the physics literature the point $\alpha = \Gamma$ is called a "second-order phase transition" point. Examination of the friction term in Eq. (2.3) shows that there is another "phase transition" leading to the onset of oscillations with critical point $\alpha = 1$. The two critical points coincide at $(\alpha, \Gamma) = (1,1)$. In the bifurcation theory literature this critical point is often referred to as the "nilpotent linear part" or the "Takens-Bogdanov codimension-2 singularity" (see Fig. 4 and Chap. 7 of Guckenheimer and Holmes [10]).

When $\mu \neq 0$ we have, in regards to the steady-state problem, the same situation as for our first nonlinear circuit above. Now the equilibrium manifold is given by
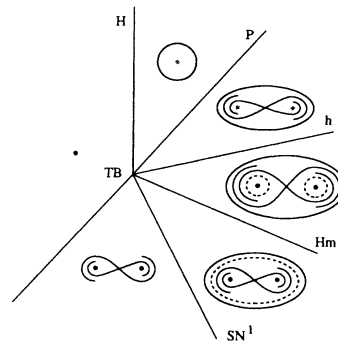
$$X^3 - (\alpha - \Gamma)X + \mu = 0 \tag{2.5}$$

FIG. 4. Bifurcation set unfolding a Takens-Bogdanov point with $\mathcal{Z}_2$ symmetry. Crosses are saddle points, black (gray) dots are stable (unstable) steady states, and solid (dashed) loops are stable (unstable) limit cycles.

and the region where F has a double well is inside the cusped sheet

$$\left(\frac{\mu}{2}\right)^2 = \left(\frac{\alpha - \Gamma}{3}\right)^3. \tag{2.6}$$

In addition to steady states we also have oscillations. The coincidence of steady-state and Hopf bifurcations now occur to yield a TB *cusp*.

C. A cross-shaped diagram

A complete picture of the bifurcation set of system (2.1) is given by showing that this system is equivalent to a class of models of chemical reactors described by Guckenheimer [13] and used by him to correct some features in Boissonade and De Kepper's "cross-shaped diagram" [14]. The cross-shaped diagram derives its name from the crossing of two curves in the (μ, Γ) plane which divides the plane into regions with oscillations, one stable steady state and bistable steady states. The cross-shaped diagram was used by Boissonade and De Kepper to summarize some general relationships between bistability and oscillations for chemical reactions in continuously stirred tank reactors. They introduced model (2.2), where X and Y denote concentrations of chemical species, as a schematic representation of circumstances where a reactor which has two stable steady states can become oscillatory.

For ease of exposition we proceed by giving a summary of Guckenheimer's analysis. System (2.2) commutes with the action of the group $\mathcal{Z}_2$,

$$(X, Z) \mapsto (-X, -Z)$$

if and only if $\mu = 0$. In this symmetric case the steady states are

$$(X, Z) = \begin{cases} (0,0) & \text{if } \alpha \leq \Gamma \\ (0,0) \text{ and } (\pm\sqrt{\alpha - \Gamma}, \pm\sqrt{\alpha - \Gamma}) & \text{if } \alpha > \Gamma. \end{cases}$$

Thus there is a pitchfork bifurcation when α is increased past Γ. The characteristic polynomial of the linearization about the origin is $\lambda^2 + (1 - \alpha)\lambda + (\Gamma - \alpha)$. Thus
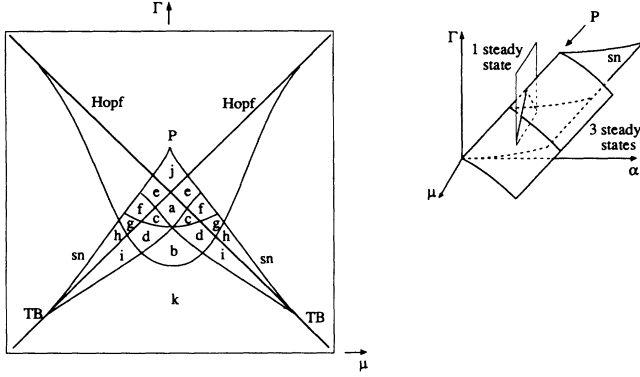
FIG. 5. Inside the box: Guckenheimer's cross-shaped diagram for system (2.2). Lower-case letters correspond to phase portraits from Fig. 13. Only regions of bistability are labeled. Other labels represent bifurcations listed in Table I. Outside the box: cusped sheet dividing the parameter space according to the number of steady states and section where the cross-shaped diagram is found.

$(0,0)$ undergoes a Hopf bifurcation when $\alpha = 1$, $\Gamma > \alpha$. There is a TB singularity at $(\alpha, \Gamma) = (1,1)$. The linearization about $(\pm\sqrt{\alpha - \Gamma}, \pm\sqrt{\alpha - \Gamma})$ has characteristic polynomial $\lambda^2 + (2\alpha - 3\Gamma + 1)\lambda + 2(\alpha - \Gamma)$. Thus the nontrivial steady states undergo a Hopf bifurcation when $2\alpha - 3\Gamma + 1 = 0$, $\alpha \geq \Gamma$. Nonlinear analysis is required for the stability calculations. These are performed in Guckenheimer's paper and the resulting bifurcation set for $\mu = 0$ is shown in Fig. 4.

To complete our picture we need to see how the bifurcation set in Fig. 4 evolves as we vary μ. It can be seen that steady-state bifurcations occur by crossing the cusped sheet (2.6) in the (α, Γ, μ) space. This bifurcation is a pitchfork if $\mu = 0$ and a fold if $\mu \neq 0$. At a fold point the state is

$$\left(\mathrm{sgn}(\mu)\sqrt{\frac{\alpha - \Gamma}{3}}, \mathrm{sgn}(\mu)\sqrt{\frac{\alpha - \Gamma}{3}}\right).$$

By linearizing about this point we find a TB bifurcation at $\Gamma = 1$. On a section of constant $\alpha > 1$ the bifurcation set is the "cross-shaped diagram" given in Guckenheimer [13] and reproduced here in Fig. 5.

III. THE SYMMETRIC SYSTEM

We now proceed with the bifurcation analysis of the chaotic Van der Pol–Duffing oscillator. Applying Kirchoff's current law to Fig. 1, we obtain the equations

$$\dot{V_1} = -\frac{1}{C_1}\left[bV_1^3 + \left(a + \frac{1}{r}\right)V_1 + \left(\nu - \frac{1}{r}V_2\right)\right],$$

$$\dot{V_2} = \frac{1}{C_2}\left[\frac{1}{r}(V_1 - V_2) - I_L\right], \qquad (3.1)$$

$$\dot{I_L} = \frac{1}{L}V_2,$$

where the variables V_1 and V_2 are voltages produced by

the circuit, I_L is the current through the inductor, C_1 and C_2 are capacitances, and r is the coupling resistor. If $\nu = 0$ this system commutes with the action of the group $\mathscr{Z}_2$,

$$(V_1, V_2, I_L) \mapsto (-V_1, -V_2, -I_L).$$

For subsequent analysis it is more convenient to rescale as follows:

$$X = \sqrt{br}V_1, \qquad Y = \sqrt{br}V_2,$$

$$Z = \sqrt{br^3}I_L, \qquad \tau = \frac{1}{rC_2}t,$$

obtaining the system in the form

$$\dot{X} = -\gamma\left[X^3 - \alpha X + (\mu - Y)\right],$$

$$\dot{Y} = X - Y - Z, \qquad (3.2)$$

$$\dot{Z} = \beta Y,$$

where differentiation is with respect to τ and the four parameters are $\alpha = -(1 + ar)$, $\beta = C_2 r^2/L$, $\mu = \sqrt{br^3}\nu$, and $\gamma = C_2/C_1$. Note that β and γ are positive by definition.

In order to understand the bifurcations of system (3.2), it is first necessary to analyze the symmetric system. Therefore in this section we set $\mu = 0$ and use local and global methods to find the bifurcation set in the (α, β, γ) space of the symmetric system

$$\dot{X} = -\gamma(X^3 - \alpha X - Y),$$

$$\dot{Y} = X - Y - Z, \qquad (3.3)$$

$$\dot{Z} = \beta Y.$$

The steady states are given by

$$S^0 = (0, 0, 0),$$

$$S^\pm = (\pm\sqrt{\alpha}, 0, \pm\sqrt{\alpha}) \qquad \text{if } \alpha > 0.$$

Thus, there is a supercritical pitchfork bifurcation giving rise to a symmetric double-well potential when α is increased past zero.

This section is divided into four subsections. The first three subsections use local methods to obtain a partial bifurcation set for system (3.3). The first subsection is concerned with a stability analysis for the symmetric system. We find a Hopf bifurcation of S^0 and give its criticality with respect to the bifurcation parameter β. There is also a Hopf bifurcation of $S^\pm$. These two Hopf lines meet the pitchfork line at a TB point with $\mathscr{Z}_2$ symmetry. In Sec. III B a reduction to a two-dimensional center manifold is performed near the $\mathscr{Z}_2$-symmetric TB point. In Sec. III C a complete description of the linearization about each steady state is given. By Glendinning and Sparrow [15], the eigenvalues of the linearization impose conditions on homoclinic orbits if they exist. For any fixed $\gamma \neq 1$, the center manifold analysis of Sec. III B proves the existence of at least one line of homoclinic orbits in the (α, β) space. Following Glendinning and Sparrow, the (α, β) space will be divided into distinct regions according to the possible types of principal homoclinic

orbits. Finally in Sec. III D we complete the bifurcation set with global results obtained from numerical investigations.

A. Stability analysis

The Jacobian matrix of system (3.3) is

$$J(X,Y,Z) = \begin{pmatrix} -\gamma\left(-\alpha + 3X^2\right) & \gamma & 0 \\ 1 & -1 & -1 \\ 0 & \beta & 0 \end{pmatrix}.$$

There is a Hopf bifurcation of S^0 corresponding to eigenvalues $\pm i\omega_1$, λ_1 where

$$\lambda_1 = \alpha\gamma - 1,$$
$$\omega_1^2 = -\alpha\gamma^2(1 + \alpha),$$

along the intersection of the parabola

$$\beta = \gamma(1 - \alpha\gamma)(1 + \alpha) \tag{3.4}$$

with the region $-1 < \alpha < 0$. In this region $\lambda_1 < 0$, and thus the system reduces to a two-dimensional center manifold near the parabola Eq. (3.4). In order to have a three-dimensional center manifold we also need $\lambda_1 = 0$. This is prohibited in the present problem since $\lambda_1 = 0$ implies $\alpha = \frac{1}{\gamma} > 0$ which contradicts the condition $-1 < \alpha < 0$.

System (3.3) has a TB bifurcation when the reduced system has a nilpotent linear part. This happens when $\omega_1 = 0$ which occurs for $(\alpha, \beta) = (0, \gamma)$ for each $\gamma > 0$. We will return to this point in Sec. III B. A TB bifurcation also occurs for $(\alpha, \beta) = (-1, 0)$. This point lies on the boundary of our domain and must be investigated by approaching the limit $\beta \to 0$. In terms of the physical parameters this limit can be achieved by taking $r \to 0$ or $C_2 \to 0$ or $L \to \infty$. We do not pursue this question further.

We now proceed with the linearization about $S^\pm$. These undergo a Hopf bifurcation, with eigenvalues $\pm i\omega_2$, λ_2 where

$$\lambda_2 = -2\alpha\gamma - 1,$$
$$\omega_2^2 = 2\alpha\gamma^2(1 - 2\alpha),$$

along the intersection of the parabola

$$\beta = \gamma(1 + 2\alpha\gamma)(1 - 2\alpha) \tag{3.5}$$

with the region $0 < \alpha < \frac{1}{2}$. Since $\lambda_2 = 0$ implies $\alpha = -\frac{1}{2\gamma} < 0$, we are again unable to obtain a three-dimensional center manifold. Note that there are double zero eigenvalues when $\alpha = 0$ or $\frac{1}{2}$; $\alpha = 0$, implying $\beta = \gamma$, coincides with the TB point found above. The case $(\alpha, \beta) = (\frac{1}{2}, 0)$ again requires an investigation of the limit $\beta \to 0$ and is not pursued further.

In order to compute the criticality of the Hopf bifurcation from S^0, we apply the coordinate change

$$\begin{pmatrix} X \\ Y \\ Z \end{pmatrix} = P \begin{pmatrix} z \\ \bar{z} \\ x \end{pmatrix}$$

such that

$$P^{-1}LP = \begin{pmatrix} i\omega_1 & 0 & 0 \\ 0 & -i\omega_1 & 0 \\ 0 & 0 & \lambda_1 \end{pmatrix},$$

where $L = J(S^0)$. Note that this preserves the $\mathscr{Z}_2$ symmetry

$$(z, x) \mapsto (-z, -x).$$

Every ordinary differential equation with this symmetry and the correct linear part is

$$\dot{z} = i\omega_1 z + c_0 z^3 + c_1 z^2\bar{z} + c_2 z\bar{z}^2 + c_3\bar{z}^3 + d_0 xz^2$$
$$+d_1 xz\bar{z} + d_2 x\bar{z}^2 + e_0 x^2 z + e_1 x^2\bar{z} + f_0 x^3 + O(5),$$
$$\dot{x} = \lambda_1 x + (h_0 z^3 + \bar{h}_0\bar{z}^3) + (h_1 z^2\bar{z} + \bar{h}_1\bar{z}^2 z)$$
$$+(j_0 xz^2 + \bar{j}_0 x\bar{z}^2) + (k_0 x^2 z + \bar{k}_0 x^2\bar{z}) + l_0 x^3 + O(5).$$

Changing coordinates once more by

$$\rho = z - \frac{c_0}{2i\omega_1}z^3 + \frac{c_2}{2i\omega_1}z\bar{z}^2 + \frac{c_3}{4i\omega_1}\bar{z}^3,$$

which also preserves the symmetry, and making $x = 0$ we get

$$\dot{\rho} = i\omega_1\rho + c_1\rho^2\bar{\rho} + O(5).$$

So the only important coefficient is $\mathrm{Re}(c_1)$ and the limit cycle created at the Hopf bifurcation is unstable or stable if $\mathrm{Re}(c_1)$ is > 0 or < 0, respectively. This is why c_1 is used to determine criticality. A straightforward calculation gives

$$\mathrm{Re}(c_1) = -\frac{3\omega_1^2\gamma^3(\gamma + 2\alpha\gamma - 1)}{2(\alpha\gamma^2 + 2\alpha\gamma - 1)}.$$

Thus $\mathrm{Re}(c_1) > 0$ or < 0 if $\alpha >$ or $< \frac{1}{2}\gamma^{-1}(1 - \gamma)$, respectively.

In Fig. 6, a partial bifurcation set in the (α, β) space summarizes these results for $\gamma \geq 1$. It shows the pitchfork P, the Hopf bifurcation H of S^0, and the Hopf bifurcation h from $S^\pm$. The point where H changes criticality with respect to the bifurcation parameter β is shown as H^c. Note that H^c exists if and only if $\gamma \geq 1$ coinciding with TB when $\gamma = 1$. This allows us to predict the existence of a critical Hopf bifurcation h^c of $S^\pm$ somewhere along the parabola h coinciding with TB and H^c when $\gamma = 1$.

When $\gamma < 1$, the phase portraits around the TB point are obtained by changing the stability of all the equilibria in Fig. 6 (see Fig. 4). In this case, the understanding of the behavior in a small neighborhood of TB is all we need. Other stable equilibria are not expected no matter how far we go from this point in the parameter space. This is why from now on we concentrate on the case $\gamma > 1$.

B. A two-dimensional center manifold

In this section we make use of results in Guckenheimer and Holmes [10] which we abbreviate here by GH.

We now turn our attention to a study of the neighborhood of the TB point $(\alpha, \beta) = (0, \gamma)$ where the lineariza-
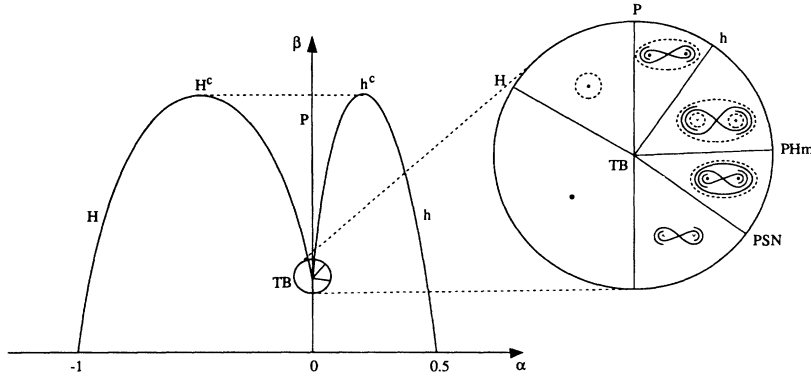
FIG. 6. Partial bifurcation set obtained by local analysis for $\gamma > 1$. H^c was computed analytically and it occurs at $(\alpha, \beta) = ((1 - \gamma)/2\gamma, (1 + \gamma)^2/4)$. h^c has not been computed but it was found numerically around $(\alpha, \beta) = ((\gamma - 1)/4\gamma, (1 + \gamma)^2/4)$. As γ decreases towards 1, both H^c and h^c move towards TB.

tion of system (3.3) about S^0 has a double zero and a negative eigenvalue. The corresponding eigenspaces are

$$E_0 = \{(X, Y, Z) | X - Y - Z = 0\},$$
$$E_{-1} = \{(X, Y, Z) | X + \gamma Y = 0, X - Z = 0\}.$$

Thus the system reduces to a two-dimensional center manifold, which is tangent to $X - Y - Z = 0$.

By GH a system with $\mathcal{Z}_2$ symmetry and a double zero eigenvalue reduces to a normal form

$$\begin{aligned} \dot{x} &= y + O(5), \\ \dot{y} &= ax^3 + bx^2y + O(5), \end{aligned} \tag{3.6}$$

in the center manifold, which in the context of $\mathcal{Z}_2$ symmetry is unfolded by

$$\begin{aligned} \dot{x} &= y + O(5), \\ \dot{y} &= \nu_1 x + \nu_2 y + ax^3 + bx^2y + O(5), \end{aligned} \tag{3.7}$$

if $a, b \neq 0$. Bifurcation sets of this normal form in the (ν_1, ν_2) space are given in Carr [16] and GH. Comparing with the partial bifurcation set in Fig. 6, we see that by a center manifold reduction we must obtain a system of the form (3.7) where $a < 0$ and b has the sign of $\gamma - 1$. Recalling that TB bifurcations occur when $\beta = \gamma$, we expect $(\alpha, \beta) = (0, 1)$ to be a degenerate TB point. A completion near TB as in GH has been included in Fig. 6 for the case $\gamma > 1$. Now we have a homoclinic bifurcation PHm, a saddle node of limit cycles PSN and the stability of the Hopf bifurcation h from $S^\pm$. There remains the question of how these results appear in a global bifurcation picture. We return to this in Sec. III D where we concentrate on the case $\gamma > 1$ since for this case numerical simulations reveal more interesting behavior.

By computing the third-order approximation of the reduced system we get

$$\begin{aligned} \dot{x} &= y + O(5), \\ \dot{y} &= -\gamma^4 x^3 + 3\gamma^3(\gamma - 1)x^2y + O(5), \end{aligned} \tag{3.8}$$

which is three-determined if and only if $\gamma \neq 1$. This confirms our prediction of a degeneracy at $\gamma = 1$. Furthermore, we can also confirm that under the imposed condition $\gamma > 0$ the only degenerate point is $(\alpha, \beta) = (0, 1)$. In order to obtain its codimension we compute the fifth-order approximation of the reduced system for $\gamma = 1$ obtaining

$$\begin{aligned} \dot{x} &= y + O(7), \\ \dot{y} &= -x^3 + 3x^5 - 9x^4y + O(7), \end{aligned} \tag{3.9}$$

which is fully determined. According to the normal form analysis in GH, this five-determined system corresponds to a codimension-3 degeneracy.

C. Restrictions on homoclinic orbits

In this section we make use of results in Glendinning and Sparrow [15] which we abbreviate here by GS.

As shown in Sec. III B by center manifold techniques, if $\gamma \neq 1$ then system (3.3) exhibits Hopf bifurcations of the three steady states, a homoclinic connection to S^0, and a saddle node of limit cycles near a TB point $(\alpha, \beta) = (0, \gamma)$. As codimension-1 bifurcations, each of these occurs along a line in the (α, β) space. Information about the Hopf bifurcation lines was given in Sec. III A, namely, their location in the (α, β) space and the stability of the created limit cycles was given. The homoclinic line will be followed in Sec. III D by numerical integration. By GS the linearization of the system about the saddle point gives information about behavior near homoclinicity. In a $\mathcal{Z}_2$ symmetry context, Glendinning [17] shows that if the Šilnikov conditions on the eigenvalues are satisfied, then infinite sequences of saddle-node, period-doubling, and symmetry-breaking bifurcations and more complicated homoclinic orbits must exist.

GS consider homoclinic orbits to steady states at which the linearization of the system has eigenvalues $-\rho \pm i\omega$, λ, where $\rho, \lambda > 0$ and ω real. They define the ratio $\delta = \frac{\rho}{\lambda}$ and describe a sequence of bifurcations obtained by varying a parameter along a line of constant δ near principal homoclinicity. A homoclinic bifurcation is of Šilnikov type if $\delta < 1$, and it involves stable or unstable orbits if $\delta > $ or $< \frac{1}{2}$ respectively. In our two-parameter system δ can be varied. Thus, results of GS apply to the two-dimensional bifurcation set in the (α, β) space by following any nonsingular bifurcation path transversal to the principal homoclinic line, and not necessarily δ=const. The numerical results in Sec. III D were obtained by fixing α and varying β. GS describe how, in two-parameter systems where δ can be varied, the sequence of bifurcations near homoclinicity may be thought of as the corresponding principal homoclinic orbit without any loss from a global point of view.

In order to check Šilnikov's condition we need to be in a region of the parameter space where the linearization $J(S^0)$ of system (3.3) about S^0 has a pair of complex conjugate eigenvalues. Denote $P(\lambda)$ as the characteristic polynomial of $J(S^0)$. This has a double eigenvalue when

$$P(\lambda) = \frac{dP(\lambda)}{d\lambda} = 0.$$

A straightforward calculation shows that this happens along the cusp

$$a_0 + a_1\beta + a_2\beta^2 + \beta^3 = 0,$$

where

$$a_0 = -\tfrac{1}{4}\gamma^2(1+\alpha)^2[(1-\alpha\gamma)^2 + 4\gamma(1+\alpha)],$$

$$a_1 = \tfrac{1}{2}\gamma[\,(1-\alpha\gamma)^2(1+\alpha) + 6\gamma(1+\alpha)^2 - 2(1-\alpha\gamma)^3\alpha$$
$$-6(1-\alpha\gamma)(1+\alpha)\alpha\gamma]$$

$$a_2 = \tfrac{1}{4}[\,-(1-\alpha\gamma)^2 - 12\gamma(1+\alpha) + 27\alpha^2\gamma^2$$
$$+3(1-\alpha\gamma)\alpha\gamma].$$

This cusped curve is schematically represented as DE (for double eigenvalue) in Fig. 7. It divides the (α, β) space into two regions according to the number of complex eigenvalues. Inside the cusp all three eigenvalues are real and outside there is a complex conjugate pair.

We also have that any given $\delta \neq \tfrac{1}{2}$ is constant along the curve

$$\beta = \frac{1 - \alpha\gamma}{2\delta\alpha\gamma - 1}\left[\frac{2\delta}{(2\delta - 1)^2}(1 - \alpha\gamma)^2 - \gamma(1 + \alpha)\right]$$

and $\delta = \tfrac{1}{2}$ if and only if $\alpha = \tfrac{1}{\gamma}$. The curves $\delta = \tfrac{1}{2}$ and $\delta = 1$ are also shown schematically in Fig. 7.

We are left with the question of where the homoclinic line goes when it leaves a small neighborhood of the TB point $(\alpha, \beta) = (0, \gamma)$. This is one of the problems addressed in Sec. III D. That information together with the analysis of the eigenvalues in this section will be enough to show the existence of Šilnikov behavior near the segment of the principal homoclinic line that is in the region $\delta < 1$.

D. Global results

So far we have used local methods of bifurcation analysis applied to system (3.3). The information obtained there will be completed here by numerical methods. More precisely, the TB bifurcations found at $(\alpha, \beta) = (0, \gamma)$ for any γ imply a line of homoclinic orbits in the (α, β) space. We now need to use global methods to determine the evolution and effects of this homoclinic bifurcation far away from the TB point. Also, given the change of criticality of the Hopf bifurcations H and h, we expect, in the (α, β) space, lines where the created limit cycles undergo saddle-node bifurcations. These lines meet H and h at H^c and h^c, respectively, and as global bifurcations they could not be followed by local methods in the previous sections.

In this section, results of numerical integration of model (3.3) are described. The computations were carried out using a fourth-order Runge-Kutta algorithm, and most were done on a FASTec AT&T-DSP32 based coprocessor board attached to a personal computer in single, i.e., 32-bit, precision. By this procedure we describe dynamics related to global bifurcations, namely, saddle node of limit cycles, period-doubling, and collision of attractors. Double precision calculations were used as a check on selected bifurcations.

All the results will be presented in the (α, β) space for fixed values of γ. Also here we assume $\gamma > 1$ for the reasons stated before. The value $\gamma = 100$ will be used in this section.

The homoclinic bifurcation PHm whose existence was proved near $(\alpha, \beta) = (0, \gamma)$ by center manifold techniques and results in Carr and Guckenheimer and Holmes has been followed. Results for the location of this principal homoclinic line in the (α, β) space are shown in Fig. 8. Also shown in the figure for comparison are the results of the analysis of the linearization at S^0 given in Sec. III C. We see that the homoclinic line crosses the cusp DE (double eigenvalue) where a pair of eigenvalues changes from real to complex conjugate.

Figure 8 also shows the principal homoclinic line going into the region where the Šilnikov condition $\delta < 1$ is satisfied. By Glendinning [17] this implies infinite sequences of saddle node of limit cycles, period-doubling
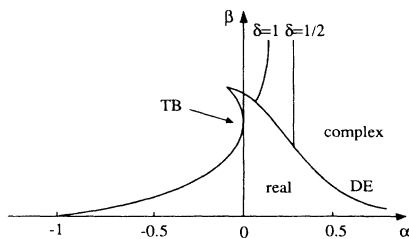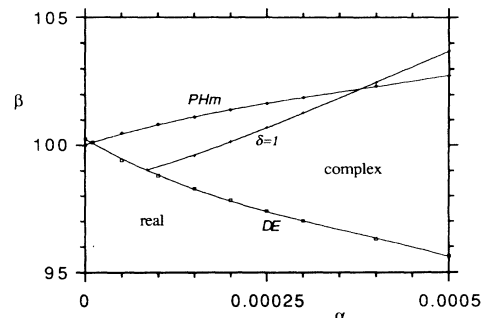
FIG. 7. Critical eigenvalue curves. $J(S^0)$ has a pair of complex conjugate eigenvalues outside the cusped curve DE. If there is a homoclinic bifurcation to S^0 in the subregion outside DE where $\delta < 1$ (to the right of $\delta = 1$) this bifurcation is of the Šilnikov type. In the region $\tfrac{1}{2} < \delta < 1$ the limit cycles are expected to be of arbitrarily large period near homoclinicity, and in the region $0 < \delta < \tfrac{1}{2}$ the limit cycles are expected to be unstable.

FIG. 8. Principal homoclinic line to S^0. There is a homoclinic bifurcation to S^0 by crossing the line PHm. It goes into the Šilnikov region (above DE and to the right of $\delta = 1$).
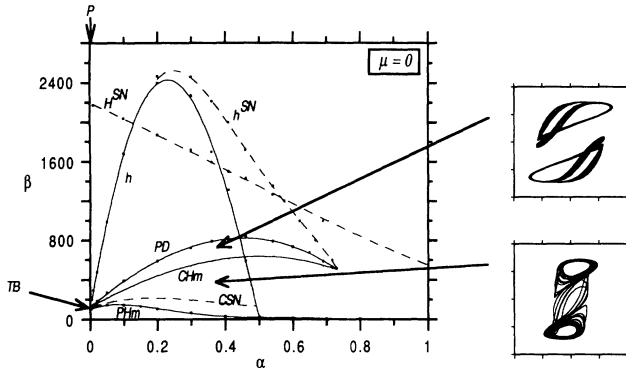
FIG. 9.   Bifurcation set at $\gamma = 100$ and $\mu = 0$. The attractors before and after a symmetry-increasing bifurcation are also shown. Before the symmetry-increasing bifurcation $(\alpha, \beta) = (0.35, 700)$ and after $(\alpha, \beta) = (0.35, 300)$.

FIG. 10.   Principal homoclinic lines to S^0 and $S^\pm$. The homoclinic line PHm to S^0 meets the TB point. The homoclinic line nHm to $S^\pm$ does not meet this point.

and symmetry-breaking bifurcations, and more complicated homoclinic orbits occuring nearby. These bifurcations occur along codimension-1 lines in the (α, β) space and therefore they are expected to cross. We have numerical evidence of a codimension-2 degeneracy when a saddle node (SN) of limit cycles and a period-doubling (PD) bifurcation undergo a PD-SN interaction. This point is not fully understood. We describe our observations here and keep the problem under investigation. Preliminary results suggest a change of stability of the period-doubling cascade. This also suggests a mechanism for the change of stability near the principal homoclinic bifurcation at $\delta = \frac{1}{2}$.

We proceed by describing some bifurcation sequences obtained by fixing α and decreasing β from a value sufficiently high to catch the whole variety of bifurcations. The line PD in Fig. 9 represents the beginning of a period-doubling cascade bifurcating from the stable limit cycles created at the Hopf bifurcation h or at the saddle node of limit cycles h^{SN} depending on the value assigned to α. A homoclinic bifurcation CHm has been found far from principal homoclinicity. This is a homoclinic bifurcation of one of the limit cycles created in the
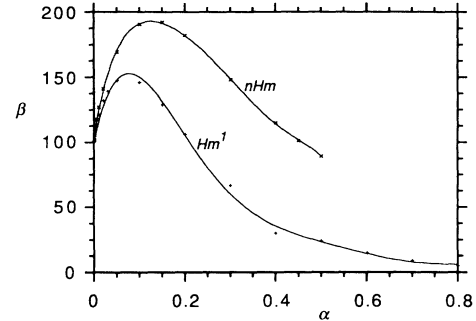
period-doubling cascade starting at PD. There is a PD-SN interaction when PD meets h^{SN}. Also CHm appears to meet this point. This homoclinic bifurcation CHm plays an important role outside the parabola of Hopf bifurcation from $S^\pm$. These steady states are sinks in that region and S^0 has a one-dimensional unstable manifold that goes into their basins of attraction. This implies that when the first homoclinic line is crossed by decreasing β, the orbit goes into one of these sinks, rather than into the large stable periodic orbit that has just been created as a result of the homoclinc bifurcation.

The stable periodic orbit obtained by the sequence of bifurcations described above dies in a saddle-node of limit cycles along the line CSN. We remark that PD, CHm and CSN do not meet the TB point $(0, \gamma)$. If they did, then this would contradict the existence of a two-dimensional center manifold. Healey et al. [3] have experimental evidence that PD folds over before getting into a sufficiently small neighborhood of TB and that it stops being observable at a PD-SN interaction.

We now have a picture of how the Hopf and homoclinic bifurcations whose occurence was shown near $(\alpha, \beta) = (0, \gamma)$ evolve as we leave a small neighborhood of that point. The saddle node of limit cycles proved to exist near $(0, \gamma)$ by a center manifold reduction in Sec. III has

TABLE I.   Notation for bifurcations.

P	pitchfork bifurcation
SN	saddle node bifurcation
H	Hopf bifurcation from S^0
h	Hopf bifurcation from $S^\pm$
H^c	degenerate H where a change of criticality occurs
TB	Takens-Bogdanov bifurcation
H^{SN}	saddle node of limit cycles created at H
h^{SN}	saddle node of limit cycles created at h
PD	period doubling of a stable limit cycle created at h or h^{SN}
PHm	principal homoclinic bifurcation to S^0
CHm	first homoclinic bifurcation to S^0 crossed by decreasing β (crisis)
nHm	homoclinic bifurcation to $S^\pm$
PSN	saddle node of limit cycles involving one created at PHm
CSN	saddle node of limit cycles involving one created at CHm

not been followed and is not included in Fig. 9. The bifurcation set now includes some behavior not associated with $(0, \gamma)$, namely PD, CHm, and CSN.

Also in Fig. 9 is the line H^{SN} where the limit cycles created at the Hopf bifurcations H from S^0 undergo a saddle-node bifurcation. The line H^{SN} meets H at a codimension-2 Hopf bifurcation H^c. This point is not shown in the figure but it can be recalled from Figure 6 which shows the analytical prediction for its location.

Homoclinicities to $S^\pm$ have also been found. Figure 10 shows a line nHm where these principal homoclinic connections occur in the (α, β) space. The principal homoclinic line to S^0 is also shown for comparision. We observe that, by the center manifold analysis in Sec. III, nHm does not meet the point $(0, \gamma)$.

The labels corresponding to bifurcations presented up to this point are listed in Table I.

IV. UNFOLDING THE DOUBLE WELL

In this section we consider the effect of the symmetry-breaking parameter μ on the results described in Sec. III. For convenience we reproduce the model here:

$$
\begin{aligned}
\dot{X} &= -\gamma(X^3 - \alpha X - Y + \mu), \\
\dot{Y} &= X - Y - Z, \\
\dot{Z} &= \beta Y.
\end{aligned}
\tag{4.1}
$$

As in Sec. III we fix γ at some value > 1. A bifurcation picture will be given on sections of the (α, β, μ) space. For each fixed β there is a steady-state bifurcation when we cross the cusped sheet $\left(\frac{\mu}{2}\right)^2 = \left(\frac{\alpha}{3}\right)^3$ as in Fig. 11 by increasing α. This bifurcation is a pitchfork if $\mu = 0$ and a saddle node if $\mu \neq 0$. The state of the system at a saddle-node bifurcation is

$$
(X, Y, Z) = \left(\mathrm{sgn}(\mu)\sqrt{\frac{\alpha}{3}}, 0, \mathrm{sgn}(\mu)\sqrt{\frac{\alpha}{3}} \right),
\tag{4.2}
$$

where $\alpha \geq 0$. Linearizing about these steady states we see that the Jacobian $J\left(\pm\sqrt{\frac{\alpha}{3}}, 0, \pm\sqrt{\frac{\alpha}{3}}\right)$ does not depend on α. So for $\mu \neq 0$ there is still a TB bifurcation at $\beta = \gamma$ but now for any (α, μ) along the cusp $\left(\frac{\mu}{2}\right)^2 = \left(\frac{\alpha}{3}\right)^3$ as in Fig. 11. Thus, for each fixed $\gamma > 0$ there is a TB cusp in the plane $\beta = \gamma$.

We recall that system (4.1) reduces to a two-dimensional center manifold near $(\alpha, \beta, \mu) = (0, \gamma, 0)$,

and that system (3.7) in Sec. III B is the normal form for the universal unfolding of the most generic $\mathcal{Z}_2$-symmetric TB singularity. In order to break completely the symmetry of the reduced system (3.7), we need the parameters (μ_1, μ_2). The nonsymmetric universal unfolding is

$$
\begin{aligned}
\dot{x} &= y + O(4), \\
\dot{y} &= \mu_1 + \mu_2 x^2 + \nu_1 x + \nu_2 y + ax^3 + bx^2 y + O(4),
\end{aligned}
\tag{4.3}
$$

if $a, b \neq 0$. This family of planar systems is described in Dangelmayr and Guckenheimer [18]. These authors divide the (μ_1, μ_2) plane into regions bounded by curves along which codimension-3 bifurcations occur. To each of these regions is associated a bifurcation set in the (ν_1, ν_2) plane. By varying the symmetry-breaking parameter μ of our system, we will be describing a line in the (μ_1, μ_2) plane. By center manifold calculations near $(\alpha, \beta, \mu) = (0, \gamma, 0)$ we see that system (4.1) reduces the normal form (4.3) with $\mu_2 = 0$. By a change of coordinates we can show equivalence with a time reverse of the
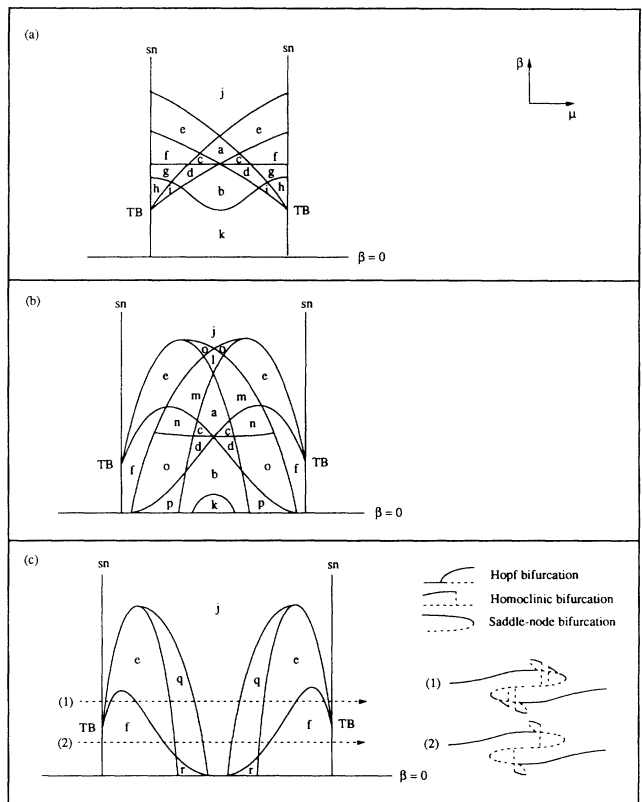
FIG. 12. Schematic sequence of bifurcation sets for fixed values of α: (a) $\alpha_1, \alpha_1 \approx 0$; (b) $\alpha_2, \alpha_2 \gg \alpha_1$; (c) $\alpha_3, \alpha_3 > \alpha_2$. See Fig. 14 for a localization of α_j in the (μ, α) plane. Lower-case letters correspond to phase portraits from Fig. 13. The bistable region of Guckenheimer's cross-shaped diagram can be obtained from (a) by joining the top of the two SN lines to form a cusped curve. In (c) we show also the bifurcation diagrams by following paths (1) and (2). These paths cross the whole region of bistability by keeping β fixed and increasing μ.
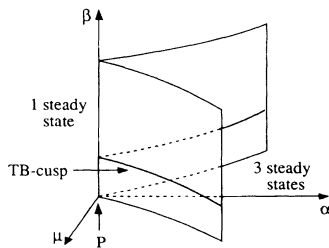

FIG. 11. Cusped sheet where steady-state bifurcations occur and TB cusp. The steady-state bifurcations are pitchforks along the line P and saddle node otherwise.
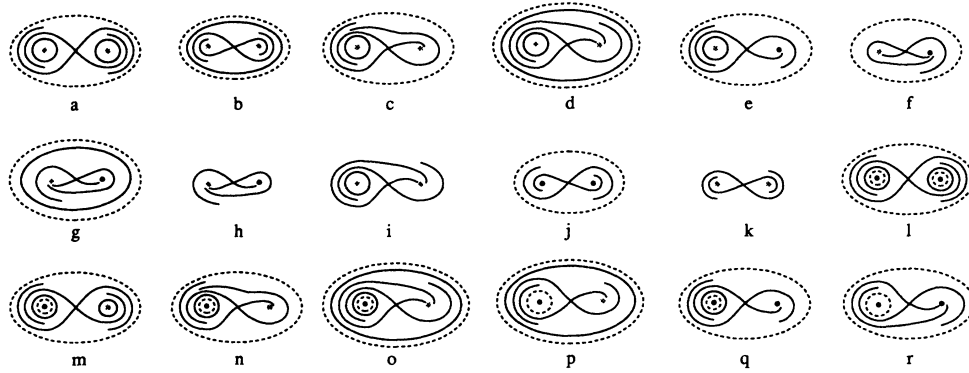
FIG. 13. Planar phase portraits corresponding to Figs. 5 and 12. Crosses are saddle points, black (gray) dots are stable (unstable) steady states, and solid (dashed) loops are stable (unstable) limit cycles.

planar Van der Pol–Duffing oscillator presented in Sec. II and fully described by Guckenheimer [13] in the context of chemical reactors. The "cross-shaped diagram" given by this author, together with the location of steady-state bifurcations obtained above, gives the bifurcation set in Figs. 12(a) obtained by fixing α arbitrarily close to zero and varying β and μ. Numerical simulations, not shown here in detail, suggest an evolution of this bifurcation set by increasing α as shown schematically in Figs. 12(b) and 12(c). By schematic representation we mean not only that the scale is not real but also that the complicated Šilnikov sequence of bifurcation is represented by the single homoclinic line Hm. A planar representation of the phase portraits in each region of Fig. 12 is given in Fig. 13. For simplicity we make the convention that $\mathcal{Z}_2$-conjugate phase portraits are equivalent. See Fig. 14 for a schematic localization of the values of α chosen in Fig. 12 relative to the cusp $(\frac{\mu}{2})^2 = (\frac{\alpha}{3})^3$.

Figure 15 shows the bifurcation set in the (α, β) space for $(\gamma, \mu) = (100, 0.01)$. Apart from the saddle node of steady states SN that has been computed analytically all the other lines were obtained by numerical simulations. A comparison with Fig. 9 shows the expected fact [expressed in the diagram of Fig. 2(b) of Sec. I] that the coincidence of bifurcations from states that are conjugate by the $\mathcal{Z}_2$ symmetry in the idealization $\mu = 0$ no longer coincide when $\mu \neq 0$. On the other hand, bifurcations involving only symmetric states when $\mu = 0$ (mapped onto themselves by the symmetry) do not split into two

when $\mu \neq 0$.

One of the most remarkable phenomena observed by breaking the $\mathcal{Z}_2$ symmetry is the way that CHm splits into two lines when μ is increased from zero. We recall from Sec. III that when this line is crossed from above we observe at CHm the collision of two conjugate attractors $C^{\pm}$ with the saddle focus S^0. The result is a symmetric attractor C^0. The projection of the attractors $C^{\pm}$ and C^0 onto the (X, Z) phase space was obtained by numerical integration and the result is shown in Fig. 9. When $\mu = 0.01$ and starting from above the two lines CHm we still have two attractors but they are no longer conjugate by any symmetry. Thus there is no longer a reason that they should collide simultaneously with the saddle focus. Thus by decreasing β when we cross the first CHm only one of the attractors stops being an invariant set. By crossing the second CHm the remaining attractor collides with the saddle focus and we obtain a larger attractor that may be seen as a perturbation of C^0. A projection of the referred attractors onto the (X, Z) space is shown in Fig. 15. Again they have been obtained by numerical integration.
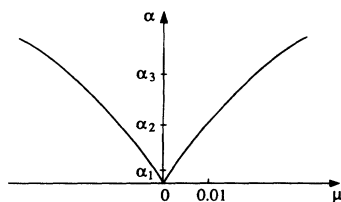

FIG. 14. Schematic localization of the sections taken in Figs. 9, 12 and 15 relative to the projection of the cusped sheet onto the (μ, α) plane.
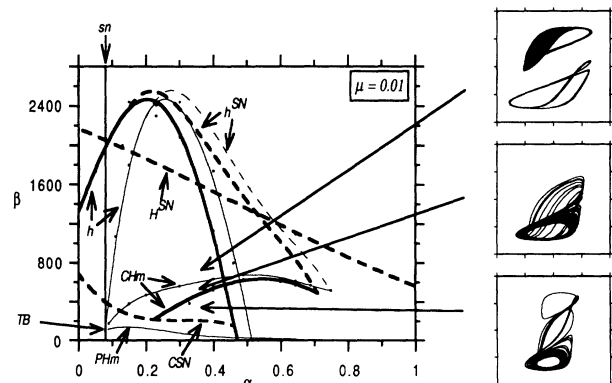

FIG. 15. Bifurcation set at $\gamma = 100$ and $\mu = 0.01$ (see Fig. 14 for a localization of $\mu = 0$ and $\mu = 0.01$). Also shown are attractors obtained from numerical simulations for parameter values $(\alpha, \beta) = (0.35, 700), (0.35, 510)$, and $(0.35, 300)$.

V. DISCUSSION AND CONCLUSIONS

We found, in a two-dimensional parameter space, a line where a Šilnikov bifurcation occurs. This line is divided into two parts: on one side we expect stable limit cycles of arbitrarily large period near homoclinicity and on the other side we expect these limit cycles to be unstable. Some of our results suggest a mechanism for this change of stability by a sequence of interactions of saddle node of limit cycles with period-doubling cascades in the wiggly curve introduced by Glendinning and Sparrow.

Stimulated by experimental observations and physical intuition derived from Ref. [4], we have studied the effect of unfolding the underlying double-well potential on the bifurcation set of a bistable chaotic oscillator. Application of this strategy yielded an example of a chaotic system with a "cross-shaped diagram" [13, 14]. We hope these results will be helpful in interpreting results from other chaotic systems that have multiple steady states (see for example, Refs. [14, 19–21]).

A natural extension of the present work is to consider a system with three potential wells. This is easily done in the present model by including quintic terms in the model for the nonlinear negative resistor. The unfolding of the quintic nonlinearity leads to the butterfly catastrophe. We have taken a brief look at some of the possible behaviors in this problem with the encouraging result that in the region of parameter space where the butterfly catastrophe shows the presence of three potential wells, chaotic trajectories that explore all three wells can be observed. We refer the reader to the paper by King and Stewart [6] where some partial results are given.

ACKNOWLEDGMENTS

[1] E. Freire, L.G. Franquelo, and J. Aracil, IEEE Trans. Circuits Syst. **CAS-31**, 237 (1984).

[2] E. Freire, A.J. Rodriguez-Luis, E. Gamero, and E. Ponce, Physica D (to be published).

[3] J.J. Healey, D.S. Broomhead, K.A. Cliffe, R. Jones, and T. Mullin, Physica **48D**, 322 (1991).

[4] G.P. King and S.T. Gaito, preceding paper, Phys. Rev. A **46**, 3092 (1992).

[5] P. Chossat and M. Golubitsky, Physica **32D**, 423 (1988).

[6] G.P. King and I.N. Stewart, in *Nonlinear Equations in the Applied Sciences*, edited by W.F. Ames and C. Rogers (Academic, London, 1992), pp. 257–315.

[7] F. Takens, Publ. Math. IHES **43**, 47 (1974).

[8] F. Takens, Comm. Math. Inst. Rijkuniversiteit Utrecht **3**, 1 (1974).

[9] R.I. Bogdanov, Funct. Anal. Appl. **9**, 144 (1975).

[10] J. Guckenheimer and P. Holmes, *Nonlinear Oscillations, Dynamical Systems and Bifurcations of Vector Fields*, Applied Mathematical Sciences Series Vol. 42 (Springer-Verlag, New York, 1986).

[11] P.T. Saunders, *An Introduction to Catastrophe Theory* (Cambridge University Press, Cambridge, 1980).

[12] E.C. Zeeman, *Catastrophe Theory: Selected Papers 1972–1977* (Addison-Wesley, Reading, MA, 1977).

[13] J. Guckenheimer, Physica **24D**, 1 (1986).

[14] J. Boissonade and P. De Kepper, J. Phys. Chem. **84**, 501 (1980).

[15] P. Glendinning and C. Sparrow, J. Stat. Phys. **35**, 645 (1984).

[16] J. Carr, *Applications of Centre Manifold Theory*, Applied Mathematical Sciences Series Vol. 35 (Springer-Verlag, New York, 1981).

[17] P. Glendinning, Phys. Lett. **103A**, 4 (1984).

[18] G. Dangelmayr and J. Guckenheimer, Arch. Rational Mech. Anal. **97**, 4 (1987); **97**, 321 (1987).

[19] D. Coles, J. Fluid Mech. **21**, 385 (1965).

[20] J. G. Charney and J. G. DeVore, J. Atmos. Sci. **36**, 1205 (1979).

[21] J. E. Hart, J. Fluid Mech **214**, 437–454 (1990); F. Cattaneo and J. E. Hart, Geophys. Astrophys. Fluid Dyn. **54**, 1 (1990).